Land–Atmosphere Coupling at the Southern Great Plains Atmospheric Radiation Measurement (ARM) Field Site and Its Role in Anomalous Afternoon Peak Precipitation

HYO-JONG SONG

Atmospheric Sciences Research Center, University at Albany, State University of New York, Albany, New York

CRAIG R. FERGUSON

Atmospheric Sciences Research Center, University at Albany, State University of New York, Albany, and Department of Environmental Resources Engineering, State University of New York College of Environmental Science and Forestry, Syracuse, New York

JOSHUA K. ROUNDY

Department of Civil, Environmental and Architectural Engineering, University of Kansas, Lawrence, Kansas

(Manuscript received 24 March 2015, in final form 24 September 2015)

ABSTRACT

The multimodel Global Land–Atmosphere Coupling Experiment (GLACE) identified the semiarid Southern Great Plains (SGP) as a hotspot for land–atmosphere (LA) coupling and, consequently, land-derived temperature and precipitation predictability. The area including and surrounding the U.S. Department of Energy Atmospheric Radiation Measurement (ARM) SGP Climate Research Facility has in particular been well studied in the context of LA coupling. Observation-based studies suggest a coupling signal that is much weaker than modeled, if not elusive. Using North American Regional Reanalysis and North American Land Data Assimilation System data, this study provides a 36-yr (1979–2014) climatology of coupling for ARM-SGP that 1) unifies prior interdisciplinary efforts and 2) isolates the origin of the (weak) coupling signal. Specifically, the climatology of a prominent convective triggering potential–low-level humidity index ($CTP–HI_{low}$) coupling classification is linked to corresponding synoptic–mesoscale weather and atmospheric moisture budget analyses. The $CTP–HI_{low}$ classification defines a dry-advantage regime for which convective triggering is preferentially favored over drier-than-average soils as well as a wet-advantage regime for which convective triggering is preferentially favored over wetter-than-average soils. This study shows that wet-advantage days are a result of horizontal moisture flux convergence over the region, and conversely, dry-advantage days are a result of zonal and vertical moisture flux divergence. In this context, the role of the land is nominal relative to that of atmospheric forcing. Surface flux partitioning, however, can play an important role in modulating diurnal precipitation cycle phase and amplitude and it is shown that soil moisture and sensible heat flux are significantly correlated with both occurrence and intensity of afternoon peak precipitation.

1. Introduction

The diurnal cycles of air temperature, clouds (humidity), and precipitation are fundamental yet complex features of regional weather and climate. They must be accurately modeled in order to capture the persistence of drought and prolonged wet events. A model with premature convective triggering (i.e., precipitation that is too frequent, too light, and peaks during daytime; e.g., Ruane and Roads 2007; Sun et al. 2006), for example, will tend to artificially lock in dry conditions because of increased infiltration and reduced runoff, enhanced evapotranspiration, and accelerated drying (Entekhabi et al. 1996; Seneviratne et al. 2006). The predictability of diurnal cycles in meteorological parameters is constrained by the highly variable land–atmosphere (LA) interactions (Ek and Mahrt 1994, their Fig. 1) that underlie them.

Corresponding author address: Craig R. Ferguson, Atmospheric Sciences Research Center, University at Albany, State University of New York, 251 Fuller Rd., CESTM-L122, Albany, NY 12203.
E-mail: crferguson@albany.edu

DOI: 10.1175/JHM-D-15-0045.1

LA coupling refers to the strength at which anomalies in local (10–100 km) land states (e.g., soil moisture and surface skin temperature) feed back on local- to regional-scale climate via surface flux partitioning [for a review, see Seneviratne et al. (2010)]. The overarching concept is that the land serves as both the source and sink of atmospheric variability. The precise sign and magnitude of the coupling varies spatially from local (5–10 km) to regional scales (400 km; e.g., Hohenegger et al. 2009) and temporally from daily to weekly time scales (Betts 2004; Koster et al. 2003; Taylor and Ellis 2006), modulated by background synoptic weather (i.e., convergence–divergence, monsoons, and cloud fields) and larger-scale (i.e., ocean–atmosphere) dynamics. During periods of weak synoptic forcing, the influence of the local (10–100 km) land state can be particularly strong. The strongest manifestation of LA coupling is convective rainfall triggering, or soil moisture–precipitation (SM–*P*) feedback. In their seminal work, Findell and Eltahir (2003) used daytime [0600–2000 Central Standard Time (CST)] precipitation as the objective criterion for fixing coupling regime classification thresholds.

The LA coupling process chain (e.g., Santanello et al. 2011) is initiated via the sensitivity of surface turbulent heat fluxes to SM. Variations in sensible and latent heat fluxes (SH and LH, respectively) at the land surface, and their interplay with free atmospheric conditions at the top of the planetary boundary layer (PBL), in turn affect near-surface thermodynamics and stability, as well as cloud and PBL heights (Betts 1992, 2009; Ek and Holtslag 2004; Santanello et al. 2007, 2009, 2011; Wood 1991). Under so-called dry-advantage conditions, strong sensible heating may trigger convection by raising the PBL to the level of free convection (LFC; Gentine et al. 2013). Wetzel et al. (1996), in a study in the Oklahoma area, found that cumulus clouds form first over drier, more sparsely vegetated areas. Similarly, Westra et al. (2012) reported observational evidence of moistening at the PBL top over dry soils near Niamey, Niger, during the 2006 African Monsoon Multidisciplinary Analyses (AMMA) intensive observational campaign. And last, a 9-yr global study conducted by Taylor et al. (2012) using satellite remote sensing microwave soil moisture and precipitation estimates revealed a widespread tendency for enhanced afternoon precipitation over drier soils, particularly over Africa and Australia.

Under so-called wet-advantage conditions, strong latent heating (and decreased sensible heating) can trigger convection by lowering the PBL height and increasing PBL moist static energy (MSE). If the LFC and lifting condensation level (LCL) are lowered far enough, then they will meet the PBL top and trigger convection (Aires et al. 2014; Findell and Eltahir 2003). Findell et al. (2011) showed that high evaporation rates in moisture-rich areas east of the Mississippi River and in Mexico increased the probability of afternoon rainfall. The LA coupling process chain is the reason why SM initialization can improve surface air temperature and precipitation short- (i.e., 12–60 h; Kumar et al. 2008; Peters-Lidard et al. 2007; Santanello et al. 2011) to long-range seasonal forecast skills [Global Land–Atmosphere Coupling Experiment, version 1 (GLACE-1; Koster et al. 2004); Global Land–Atmosphere Coupling Experiment–Coupled Model Intercomparison Project (GLACE-CMIP; Seneviratne et al. 2013); and Global Land–Atmosphere Coupling Experiment, version 2 (GLACE-2; van den Hurk et al. 2011)].

Ten years ago, the Global Energy and Water Cycle Experiment (GEWEX; http://www.gewex.org/) GLACE (Guo et al. 2006; Koster et al. 2004, 2006) spotlighted the Southern Great Plains (SGP) for being one of three hotspots globally for land-derived precipitation predictability. Since then, the GLACE results have served as the underlying motivation for numerous subsequent LA coupling studies over the SGP domain. What makes the SGP a prime region for SM–*P* feedbacks is the heightened sensitivity of the region's shallow-rooted vegetation, and thus, surface heat fluxes, to SM constraints coupled with the fact that the magnitude of the related surface heat flux changes are substantial enough to have an effect on precipitation (e.g., Dirmeyer 2011). Local point-scale studies have been carried out for the U.S. Department of Energy (DOE) Atmospheric Radiation Measurement (ARM) Southern Great Plains (hereafter, ARM-SGP; Mather and Voyles 2013) Climate Research Facility using surface meteorological and surface flux measurements for periods of 4 (Dirmeyer et al. 2006) and 12 years (Phillips and Klein 2014). Regional pentad- to monthly-scale moisture budget analyses have been carried out using atmospheric reanalysis and ARM-SGP observations for periods of 4 (Lamb et al. 2012) and 7 years (Ruiz-Barradas and Nigam 2013). A synoptic-dynamic analysis of afternoon precipitation frequency was conducted using atmospheric reanalysis for a period of 10 years (Ford et al. 2015a). Finally, regional limited-duration (2–7 days) coupled Weather Research and Forecasting (WRF) Model sensitivity experiments have been conducted (i.e., Erlingis and Barros 2014; Santanello et al. 2009, 2011, 2013a,b).

A gap analysis of these prior studies reveals the need for an analysis using multidecadal data that will 1) place the climatology of daily regional LA coupling in the context of daily synoptic-scale weather and 2) provide a comprehensive characterization of the LA coupling contribution to variations in the diurnal cycle of precipitation. This study was designed to meet this need.

Specifically, we adopt a multiscale approach that integrates a local-scale (50–400 km) land perspective with a synoptic-scale (~1000 km) atmospheric perspective to provide a unique and comprehensive characterization of dry- and wet-advantage land–atmosphere coupling events in the SGP.

This study is organized as follows. First, a climatology of land–atmosphere coupling over the SGP is compiled for the most recent 36 years (1979–2014) in the context of the convective triggering potential–low-level humidity index (CTP–HI_{low}) classification framework from Findell and Eltahir (2003). The framework distinguishes between atmospheric conditions for which convective initiation occurs preferentially according to soil moisture dry or wet anomalies (dry or wet advantage), as well as those conditions for which the role of land is negligible. Second, the coupling climatology is reinterpreted through the perspective of composite weather maps and regional atmospheric moisture budget analyses to understand in a broader context the synoptic conditions responsible for sustaining dry- and wet-coupling regimes, respectively. Third, the coupling climatology is interrogated for a local land-driven afternoon peak precipitation signal, a critical underpinning of the CTP–HI_{low} classification framework. This activity highlights characteristics that distinguish afternoon peak precipitation days from climatology, which in the SGP is nocturnal peak precipitation. Note that climatologically the SGP has a nocturnal precipitation peak. Finally, a search is conducted among 17 common convection, surface flux, and mesoscale environmental variables, for a morning-to-noon variable subset that can explain same-day afternoon peak precipitation occurrence and intensity. This search will address whether afternoon peak precipitation occurrence and intensity are predictable at short range (i.e., 8–13 h). While several variables may explain afternoon peak precipitation occurrence and intensity, this study is explicitly focused on identifying the strongest explanatory variables in coupled land–atmosphere environments.

2. Data and methods

The study region is a 4.5° latitude (500 km) × 4.5° longitude (405 km) box (34.35°–38.85°N, 95.25°–99.75°W) centered on the ARM-SGP Climate Research Facility in Lamont, Oklahoma (36.6°N, 97.5°W). The region is semiarid and spans a west–east gradient in annual precipitation from 74 to 98 cm yr^{-1} (Fig. 1a). The SGP is recognized as one of the GLACE (Guo et al. 2006; Koster et al. 2004, 2006) top three "hotspots" globally for land–atmosphere coupling (i.e., land-derived weather predictability). Climate projections for the region include earlier and shorter springs, longer and drier summers (Hidalgo et al. 2009; Melillo et al. 2014; Stewart et al. 2004), and enhanced land–atmosphere coupling (Dirmeyer et al. 2013). In this study, we focus temporally on the warm season, May–September (MJJAS), during the 36-yr period from 1979 to 2014.

We use hourly precipitation, surface (0–10 cm) soil moisture, and surface sensible and latent heat flux estimates from phase 2 of the 0.125° North American Land Data Assimilation System (NLDAS-2) primary forcing dataset (P; Xia et al. 2012) and Noah model output dataset (SM, SH, and LH; Ek et al. 2003). NLDAS-2 P is temporally disaggregated into hourly fields from the U.S. Climate Prediction Center (CPC) Parameter-Elevation Regressions on Independent Slopes Model (PRISM)-adjusted (Daly et al. 1994, 2008) 0.125° daily gauge-only P analysis by Weather Surveillance Radar-1988 Doppler (WSR-88D)-based P; 8-km CPC morphing technique (CMORPH; Joyce et al. 2004) P; or North American Regional Reanalysis (NARR; Mesinger et al. 2006)-simulated P, based on availability (in order). All other data are taken from the 3-hourly, 32-km, 29-pressure-level NARR. Specifically, the following convection-related metrics are computed from NARR for a parcel with maximum equivalent potential temperature below 3000 m above ground level (AGL): convective available potential energy (CAPE), convection inhibition (CIN), LCL, and LFC (Colman 1990). To investigate the atmospheric preconditioning of LA coupling by the synoptic environment, we analyze NARR: total column–integrated precipitable water vapor (PWV), 975–700-hPa (hereafter, low level) atmospheric moisture budget, 850-hPa geopotential height z_g, 850-hPa meridional wind v_{850}, specific humidity q at 850 hPa, and the 850–700-hPa environmental lapse rate, the rate of change of temperature T with height z between 850 and 700 hPa (dT/dz). For reference, Frye and Mote (2010) classified a day as stable or synoptically benign if 850–700-hPa dT/dz was less than 6.0 K km^{-1} and unstable or synoptically primed otherwise. Frye and Mote (2010) also used a 12 m s^{-1} 1200 UTC (0600 CST) 850-hPa wind speed threshold to determine the presence of the Great Plains low-level jet (LLJ; e.g., Bonner 1968; Stensrud 1996).

LLJs occur on 25%–50% of June–August (JJA) days (Song et al. 2005) and represent the principal mechanism by which moist and unstable air from the Gulf of Mexico is advected hundreds of kilometers northward into the Great Plains, where it ultimately becomes precipitation (e.g., Helfand and Schubert 1995; Higgins et al. 1997). Ford et al. (2015a) found that afternoon precipitation falls preferentially over wet soils when the LLJ is absent and preferentially over dry soils when the LLJ is present. We use 0600 UTC (0000 CST) v_{850} in this study because we believe it best captures the 0100–0400 CST

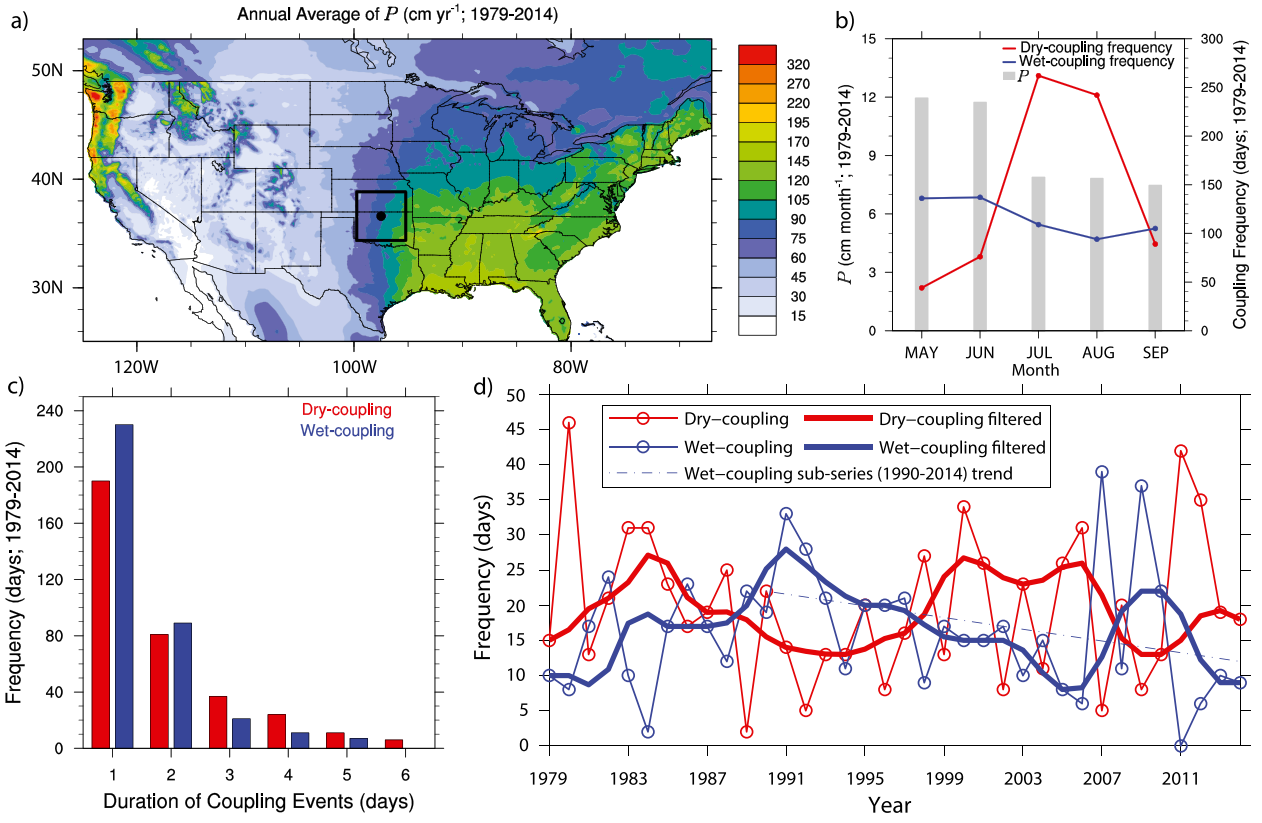

FIG. 1. (a) The SGP study domain, a 4.5° × 4.5° box centered on the ARM-SGP Climate Research Facility (36.6°N, 97.5°W; black dot), overlaid on a map of annual mean P (cm yr^{-1}) computed for the period 1979–2014 using NLDAS-2. (b) Monthly P (cm month^{-1}; gray bars), wet-coupling frequency (blue line), and dry-coupling frequency (red line) for the period 1979–2014. (c) Frequency distribution of coupling event duration (days) for the period 1979–2014. (d) Annual warm-season wet- and dry-coupling event day totals, their filtered time series (3RSSH, twice; Tukey 1977), and the 1990–2014 wet-coupling trend line (slope of −0.45 days yr^{-1} and rejection probability of 0.10).

LLJ peak southerly winds (Song et al. 2005). Additionally, we compute a nocturnal low-level jet (NLLJ) index, following Rife et al. [2010, their Eq. (1)]. The NLLJ quantifies the degree of vertical and temporal variation in wind speeds between approximately 500 and 4000 m AGL (taken as 925 and 600 hPa, respectively) and local midnight and local noon.

The other metrics (above) are considered at 0600 CST, consistent with the time of CTP–HI$_{low}$ coupling classification, with the exception of radiation-related metrics: SH, LH, net available radiation (A = SH + LH), and evaporative fraction (EF = LH/A), which are not reliably stable until 1200 CST. NLDAS-2 and NARR variables are regridded from their native resolutions to 0.5°. Unless otherwise noted, all referenced values are SGP domain-averaged quantities and statistical significance is evaluated on the basis of a two-tailed Student's t test at the 95% confidence level.

At large scales, there is little difference between the NARR and NLDAS-2 P because NARR assimilates similar gauge data sources (Mesinger et al. 2006). However, surface water and energy partitioning (i.e., runoff ratio and evaporative fraction) can vary substantially between NARR, which uses an earlier version of Noah (version 2.6), and NLDAS-2 Noah, which uses an improved version (version 2.8; e.g., Sheffield et al. 2012; Smith et al. 2012; Wei et al. 2013). For this reason, NLDAS-2 Noah is used for surface and near-surface states and fluxes. Because of the assimilation of upper-air observations and the limited time memory (relative to the land surface) of the atmospheric column, we hold that any surface-driven atmospheric inconsistencies due to NLDAS-2 Noah–NARR mismatches are minimized.

The LA coupling state for each day during the study period is classified according to a CTP–HI$_{low}$ framework (Findell and Eltahir 2003). The framework was first modified by Ferguson and Wood (2011) for global application using satellite remote sensing, and Roundy et al. (2013) subsequently improved the framework's representation of daily spatiotemporal variability in the CTP–HI$_{low}$ state space by incorporating regional historic CTP–HI$_{low}$–SM relationships. The Roundy et al.

(2013) approach is currently the most refined of the CTP–HI_{low} classification approaches, and therefore, it is the one applied here. CTP ($J\,kg^{-1}$) is defined by the integral of the area between the temperature sounding and a moist adiabat originating at 100 hPa AGL and extended up to 300 hPa AGL. The variable HI_{low} (K) is the sum of the dewpoint depressions at 50 and 150 hPa AGL. CTP and HI_{low} are calculated at 1200 UTC (0600 CST) using native NARR data and upscaled to 0.5° resolution, the scale at which coupling classification is carried out. A given day is classified as wet or dry coupling only if all grid points within the 4.5° × 4.5° SGP study domain are classified accordingly (i.e., complete spatial coherence); otherwise, the day is classified as uncoupled. This approach yields a conservative time series of coupling in the SGP that is likely to be consistent with other modern reanalyses.

The dry-coupling regime is typified by drier soils and larger CTP, which tend to support low-level CAPE. In contrast, for the wet-coupling regime, characterized by low HI_{low} and wet soils, afternoon convective initiation may follow from enhanced low-atmosphere moisture saturation. For context, 90% of wet-coupling days fall in the CTP–HI_{low} range from −55 to 171 $J\,kg^{-1}$ and 2.3 to 10.5 K, and 90% of dry-coupling days fall in the CTP–HI_{low} range from 70 to 273 $J\,kg^{-1}$ and 15.4 to 32.1 K. When classification is not uniform over the domain, 90% of the remaining days fall in the CTP–HI_{low} range from −271 to 213 $J\,kg^{-1}$ and 5.1 to 30.9 K. A fundamental expectation for coupling days is that of locally driven (unforced) afternoon convective triggering (Findell and Eltahir 2003). In practice, a convention must be adopted to screen out organized precipitation (e.g., precipitation persistence; Guillod et al. 2014) from unforced convective precipitation. Hereafter, we will focus on the difference between afternoon (1400–1900 CST Day 0) and nonafternoon precipitation (0600–1300 CST Day 0 and from 2000 CST Day 0 to 0500 CST Day 1). Any day for which the afternoon-averaged precipitation exceeds that of the nonafternoon-averaged precipitation by 0.01 $mm\,h^{-1}$ or more is deemed an afternoon peak (AP) day. As an aside, 0.01 $mm\,h^{-1}$ is the 33rd percentile of the probability distribution of all afternoon–nonafternoon precipitation differences. The hours of 1400–1900 CST are distinguished from the remainder of the day because, during these hours, precipitation on LA coupling days is correlated with 0600 CST CTP at the 95% confidence level (not shown). In the interest of clarity, we note that 1400–1900 CST precipitation corresponds explicitly to the 1300–1859 CST accumulation period.

During the period from 1908 to 2009, tropical cyclones (TCs) accounted for 26% of JJA daily extreme precipitation events in the southern United States (Texas, Oklahoma, Kansas, Arkansas, Louisiana, and Mississippi; Kunkel et al. 2012, their Fig. 5). To minimize TC impacts on our study, we omit all days for which a TC track in the second-generation Atlantic hurricane database (HURDAT2; Jarvinen et al. 1984; Neumann et al. 1999; http://www.nhc.noaa.gov/data/#hurdat) passed within 500 km of the SGP study domain. The total number of such days is 84 (or 1.5%) over the 36-yr (1979–2014) period. This study focuses on the remaining 5424 days.

In the future, the role that frontal systems play in bringing about afternoon peak precipitation should be investigated. Just as large-scale moisture transport may explain wet- and dry-coupling regime transitions, frontal weather systems may explain a portion of the afternoon precipitation peak signal. An initial investigation into this issue using subdiurnal variation in low-level (975–700 hPa) winds as a surrogate for frontal passage suggests that more fronts pass over dry-coupling afternoon peak events (not shown).

3. Results

a. *Coupling climatology and related synoptic environments*

The CTP–HI_{low}-based LA coupling climatology for the SGP domain (see Fig. 1a) is summarized in Figs. 1b–d. Of the 5424 TC-free days (see section 2), the number of wet- and dry-coupling days are 581 and 713, respectively. The seasonal distribution of these coupling days is illustrated in Fig. 1b relative to the monthly precipitation climatology. Dry-coupling days occur mainly in July and August, following a sharp mid-June climatological downturn in daily rainfall totals, referred to as the setup of the ''death ridge'' (Basara et al. 2013). The frequency of wet-coupling days, on the other hand, is more uniformly distributed, with relatively higher occurrence frequencies earlier in the warm season, during May and June.

Figure 1c illustrates the duration (days) frequency distribution for all wet- (n = 362) and dry-coupling events (n = 356) in the warm season, truncated at 6 days for succinctness. Note that the majority of coupling events are short lived; 88% and 76% of wet- and dry-coupling events, respectively, span 2 days or less. However, in general, it is more likely for 1- or 2-day coupling events to be in wet coupling and for longer-lived events to be in dry coupling. For example, 24% (n = 85) of dry-coupling events are 3 days or longer, compared to only 12% (n = 43) of wet-coupling events. There were four wet-coupling events and six dry-coupling events that exceeded 6 days in duration. The longest recorded wet- and

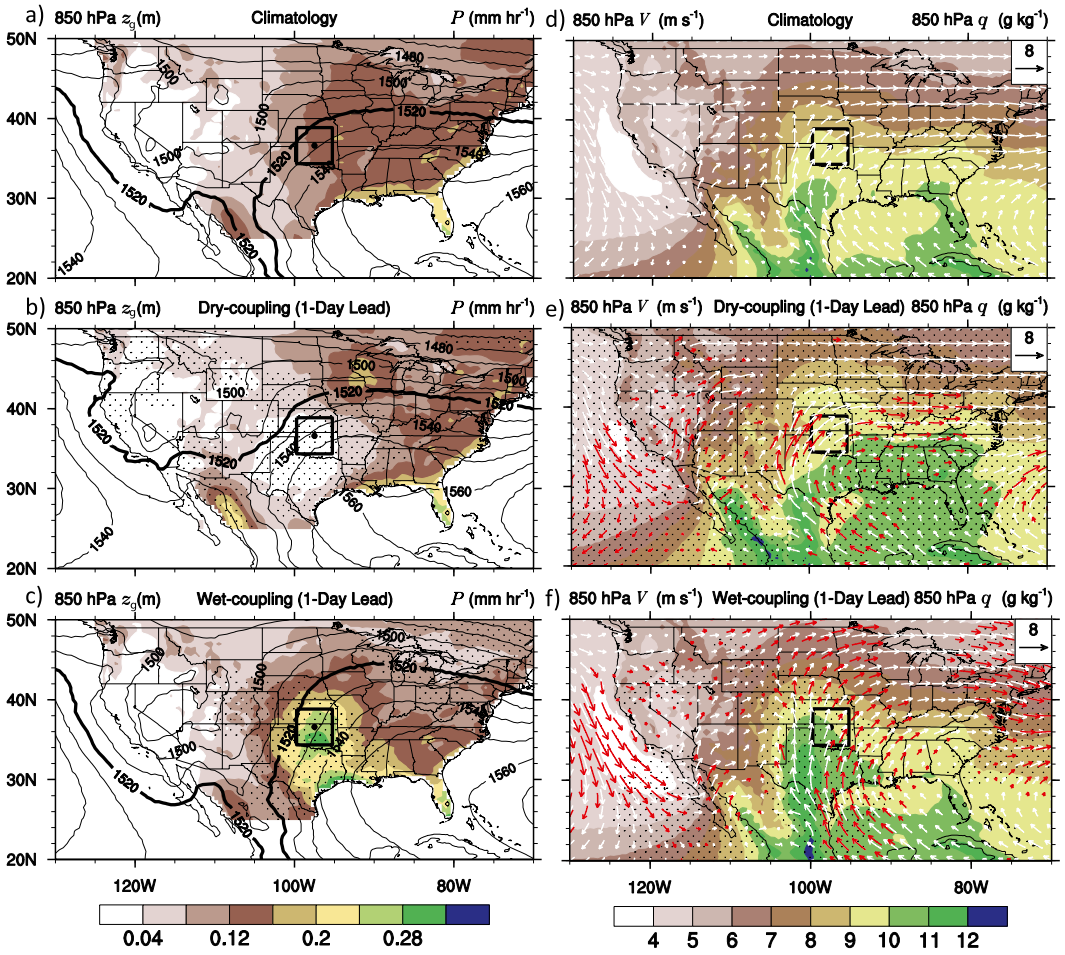

FIG. 2. Composite maps of (a)–(c) NLDAS-2 P (shading) and NARR 850-hPa z_g (contours) and (d)–(f) NARR 850-hPa q (shading) and 850-hPa V (vectors), averaged over the 24-h period from 0600 CST Day 1 to 0500 CST Day 0, which corresponds to the period immediately preceding coupling classification at 0600 CST. All warm-season days are included in the climatology composites in (a) and (d). The coupling regime determination (i.e., wet or dry coupling) is made according to the conditions over the SGP domain only (black box). For shaded variables, dots denote variations from climatology significant at the 95% confidence level. For vectors, the color red denotes differences from climatology significant at the 95% confidence level.

dry-coupling events were 10 and 15 days, respectively (not shown).

Figure 1d illustrates the year-to-year variability in wet- and dry-coupling frequencies. A "3RSSH, twice" smoother (Tukey 1977) was used to highlight low-frequency variability in the two time series. The smoother consists of a running median of three (3R), two splitting operations (SS), each of which is followed by a 3R, and Hanning (H). The smooth of the first pass is then re-roughed by adding the smooth of a 3RSSH applied to its residuals. While no statistically significant breakpoints (Pettitt 1979) exist in either full record, an iterative search of all subrecord lengths extending backward in time from 2014 revealed a decline in wet-coupling frequency at the rate of 0.45 days yr^{-1} over the last 25 years (1990–2014) significant at the 90% confidence level. The persistence of this trend should continue to be monitored over the coming years.

Through composite analyses, the synoptic-scale environments supportive of SGP wet- and dry-coupling regimes may be generalized relative to climatology (Fig. 2). Specifically, Fig. 2 shows composites of coupling event lead day (i.e., from 0600 CST Day −1 to 0500 CST Day 0) 850-hPa geopotential height and precipitation (Figs. 2b,c) and 850-hPa meridional wind and 850-hPa specific humidity (Figs. 2e,f) relative to climatology (Figs. 2a,d). The composites show that days preceding dry coupling are typified by the presence of a high pressure system at 850 hPa over the southeastern United States (Fig. 2b), which supports southwesterlies and westerlies and thereby suppresses northward moisture transport from the Gulf of Mexico into the SGP

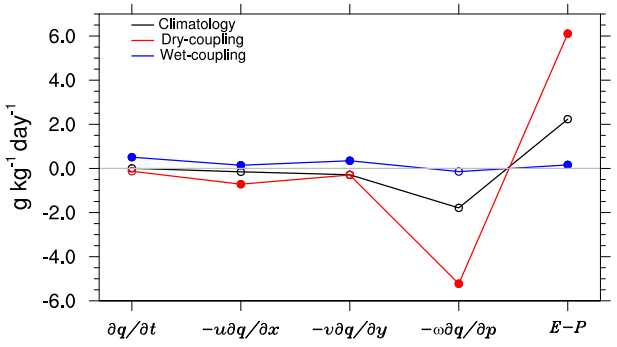

FIG. 3. Composite warm-season SGP PBL (975–700 hPa) q budget for wet coupling (blue line), dry coupling (red line), and all days (climatology; black line). From left to right, the moisture budget terms are local temporal variation ($\partial q/\partial t$), zonal convergence [$-u(\partial q/\partial x)$], meridional convergence [$-v(\partial q/\partial y)$], vertical convergence [$-\omega(\partial q/\partial p)$], and source and sink terms [evaporation (i.e., E) and precipitation (i.e., P)]. Filled circles denote differences from climatology significant at the 95% confidence level. As in Fig. 2, the budget is defined for the 24-h period immediately preceding coupling classification, or from 0600 CST Day 1 to 0500 CST Day 0.

(Fig. 2e). In contrast, days preceding wet coupling are typified by the presence of a low pressure system at 850 hPa stretching from the Rocky Mountains to the SGP, with a pronounced west–east gradient of the 850-hPa mass field (Fig. 2c). This synoptic pattern supports increased low-level horizontal moisture flux into the SGP from the south-southeast (Fig. 2f), which can act to support precipitation and, in turn, soil moistening (Figs. 2c; Aires et al. 2014).

Similarly, differences between dry- and wet-coupling regimes may be framed in terms of the time-averaged regional PBL atmospheric moisture budget (Fig. 3). The budget is defined for the volume between 975 and 700 hPa over the SGP domain ($\mathrm{PBL_{SGP}}$) by Yang et al. (2014):

$$\overline{\frac{1}{\mathrm{PBL_{SGP}}}\int_{\mathrm{PBL_{SGP}}}\frac{\partial q}{\partial t}+u\frac{\partial q}{\partial x}+v\frac{\partial q}{\partial y}+\omega\frac{\partial q}{\partial p}\,dD}=\overline{\frac{1}{\mathrm{PBL_{SGP}}}\int_{\mathrm{PBL_{SGP}}}E-P\,dD},\qquad(1)$$

where the terms on the left-hand side represent (from left to right) local temporal variation, zonal, meridional, and vertical divergence of specific humidity, and the terms of the right-hand side, evaporation E and precipitation (i.e., P), constitute moisture source and sink terms. The overbar in Eq. (1) denotes the daily average, where a day is defined from 0600 CST Day −1 to 0500 CST Day 0 (as in Fig. 2). Related variables and constants are time t, zonal velocity component u, meridional velocity component v, vertical velocity at pressure coordinate ω, and 4.5° × 4.5° SGP domain D. Figure 3 shows that as a group, days preceding wet-coupling have a significantly greater local change in the PBL specific humidity q_{PBL} ($+0.51\,\mathrm{g\,kg^{-1}\,day^{-1}}$) as well as a significantly greater horizontal moisture convergence [$-u(\partial q/\partial x) = +0.14\,\mathrm{g\,kg^{-1}\,day^{-1}}$; $-v(\partial q/\partial y) = +0.35\,\mathrm{g\,kg^{-1}\,day^{-1}}$] relative to climatology. Conversely, days preceding dry coupling have significantly enhanced zonal moisture divergence [$-u(\partial q/\partial x) = -0.71\,\mathrm{g\,kg^{-1}\,day^{-1}}$] and significantly larger losses at the entrainment layer [$-\omega(\partial q/\partial p) = -5.23\,\mathrm{g\,kg^{-1}\,day^{-1}}$] relative to climatology. The PBL budget terms during dry coupling also agree with the result of Lamb et al. (2012) in that $E - P$ is largely balanced by vertical moisture divergence. The SGP is, overall, a source region for atmospheric moisture and as a result serves as a weaker or stronger magnitude source of moisture during wet- and dry-coupling regimes, respectively (Fig. 3).

b. Coupling impacts on afternoon peak precipitation

The basis of the CTP–$\mathrm{HI_{low}}$ regime classification is that local anomalies in the land state (i.e., soil moisture) can contribute to an anomalous afternoon precipitation peak. While the climatological diurnal precipitation cycle for the SGP peaks between the hours of 0000 and 0600 CST, Fig. 4a clearly shows a temporally local AP in wet coupling and a diminished nocturnal precipitation peak in dry coupling. For the remainder of this study, we focus on dissecting these precipitation features that are sensitive to LA coupling and in particular that of the AP (defined as occurring between 1400 and 1900 CST).

In Fig. 4, the composite diurnal cycles of precipitation for various subsamples of wet- and dry-coupling events, spanning aspects of event duration (i.e., all, 2 days or longer, and 3 days or longer) and structure (i.e., day 1, 2, or 3) are presented. An enhanced afternoon precipitation peak is visually evident for all wet-coupling subsamples. However, an afternoon peak is not immediately evident for the dry-coupling samples. Accordingly, the conditional probability of AP days, notated above, is employed to determine the dry- and wet-coupling subsamples with the highest AP likelihood. They are found to be the first day of 3-days-or-longer wet-coupling events (60% AP; Fig. 4d) and the third day of 3-days-or-longer dry-coupling events (25% AP; Fig. 4f). Notably, for the 3-days-or-longer dry-coupling events, an AP centered at 1700 CST (Fig. 4c) renders the nocturnal peak insignificant at the 95% confidence level. We investigated the relatively large step shift (significant at the 99% confidence level) between 0600 and 0500 CST (on the next day) in dry-coupling samples and determined that it is attributable to differences between the average precipitation rate at 0600 on all event-start days (lower) and that at 0500 CST on all event-end days (higher).

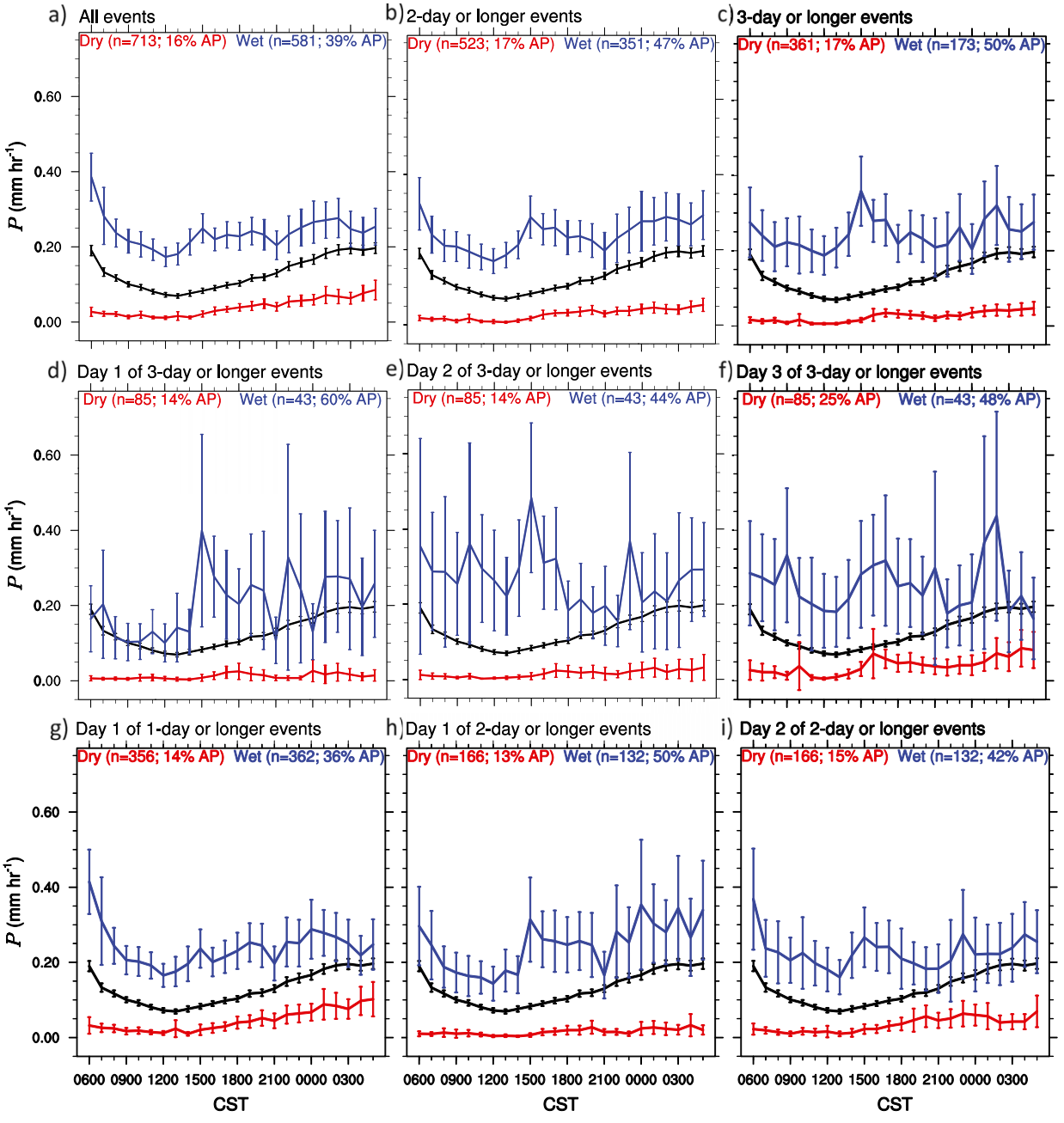

FIG. 4. Diurnal cycle of NLDAS-2 P (mm h^{-1}) over the SGP domain as a function of coupling event persistence and type (i.e., wet or dry coupling). (a) All coupling events (i.e., 1 day or longer); (b) events of 2-days-or-longer duration only; (c) events of 3-days-or-longer duration only; (d) the first day, (e) second day, and (f) third day of 3-days-or-longer events only; (g) the first day of all events; and (h) the first day and (i) second day of 2-days-or-longer events only. The warm-season climatological (i.e., all days; sample size $n = 5424$) diurnal P cycle is provided for reference (black line). Whiskers denote 95% confidence intervals. The underlying sample size (days) and the fractional composition of those days with AP precipitation is notated above.

Figure 5 provides the frequency histogram of afternoon minus nonafternoon precipitation (see section 2) for all days as well as the fraction of dry- and wet-coupling days in each 0.07 mm h^{-1} width bin. Whereas Fig. 4 shows that wet-coupling AP events are more common than dry-coupling AP events, Fig. 5 shows that their strength, or the magnitude of the difference in afternoon and nonafternoon precipitation, is also larger. In all cases, the afternoon minus nonafternoon precipitation difference in dry-coupling AP events is less than 0.14 mm h^{-1} (Fig. 5).

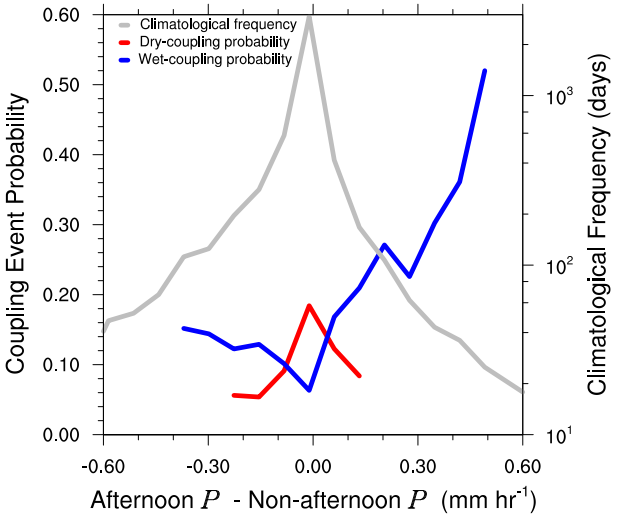

FIG. 5. Frequency distribution of daily differences between NLDAS-2 afternoon (1400–1900 CST) and nonafternoon (0600–1300 CST Day 0 and from 2000 CST Day 0 to 0500 CST Day 1) P computed for the period of 1979–2014 (gray line; right y axis). For each 0.07 mm h^{-1} bin with >10 samples, the fraction of wet- (blue line) and dry-coupling (red line) days is given (left y axis).

In other words, at values in excess of 0.14 mm h^{-1}, there is zero chance that the AP day is in dry coupling and a 20% or better chance the AP day is in wet coupling. Figure 5 shows that it is more likely that an AP event occurs outside of a coupling event, which is a potentially misleading consequence of our uniform domain classification requirement (see section 2). In fact, on a given AP day, 57% and 36% of SGP domain grids on average are classified as wet and dry coupling, respectively, meaning less than 7% of grids are classified as uncoupled or atmospherically controlled. No statistically significant trends in AP event frequency were found for either coupling regime (not shown).

c. *Factors influencing AP in coupled regimes*

The focus of the study now shifts to identifying explanatory variables for AP occurrence and magnitude in coupled LA environments. We start with a set of 17 key convective, mesoscale, and surface-flux-related variables and test whether each undergoes a mean shift between total and AP-only samples (Fig. 6). Most variables are found to undergo a significant shift in mean between total (i.e., climatology) and AP-only day samples. However, the objective is to isolate variables that capture the role of the land surface, which in this context implies statistically significant differences between both the means calculated for wet- and dry-coupling AP day subsamples relative to their wet- and dry-coupling parent samples, respectively. Only the following six variables met these criteria: 0600 CST CTP, 850–700-hPa dT/dz, LFC, 975–700-hPa layer-averaged specific humidity (i.e., q_{PBL}) and SM, and 1200 CST SH (Fig. 6). On

Variable (units)	Sample					
	All days (n=5424)	**All days w/AP (n=1104)**	Dry-coupling days (n=713)	**Dry-coupling days w/AP (n=118)**	Wet-coupling days (n=581)	**Wet-coupling days w/AP (n=230)**
0600 CST CAPE (J kg^{-1})	653.9	**708.0**	608.3	**713.6**	575.6	614.3
0600 CST CTP (J kg^{-1})	46.1	**93.4**	175.9	**207.7**	66.7	**88.7**
0600 CST 850-700-hPa dT/dz (K km^{-1})	5.9	**6.1**	7.1	**7.3**	5.5	**5.7**
0600 CST PBLH (km)	0.6	0.6	0.6	0.6	0.6	0.5
0600 CST CIN (J kg^{-1})	151.6	**116.7**	240.6	**211.3**	50.8	48.2
0600 CST LCL (km)	1.4	**1.1**	1.6	1.6	0.7	**0.6**
0600 CST LFC (km)	6.6	**4.7**	5.5	**4.3**	4.5	**3.5**
0600 CST HI_{low} (K)	15.5	**12.5**	22.7	**21.4**	6.3	6.0
0600 CST q_{PBL} (g kg^{-1})	9.6	**10.4**	9.8	**10.5**	10.8	**11.1**
0600 CST PWV (kg m^{-2})	16.8	**15.9**	17.4	17.5	16.6	15.2
1200 CST SH (W m^{-2})	211.1	**197.4**	256.2	**272.7**	167.5	**157.6**
1200 CST LH (W m^{-2})	241.1	**235.9**	227.3	**207.9**	243.7	237.9
1200 CST EF	0.5	**0.5**	0.5	**0.4**	0.6	0.6
0600 CST SM (kg m^{-2})	23.3	23.4	20.1	**19.1**	25.6	**25.1**
1200 CST A (W m^{-2})	452.2	**433.2**	483.5	480.6	411.1	**395.5**
0000 CST v_{850} (m s^{-1})	3.0	**3.6**	3.0	3.6	3.7	4.2
0000 CST NLLJ index (m s^{-1})	8.3	8.4	8.4	8.8	6.8	7.0

FIG. 6. Mean values of 17 convection and LA coupling relevant variables calculated from samples comprising (from left to right): all days, days with AP precipitation, all dry-coupling days, all dry-coupling days with AP precipitation, all wet-coupling days, and all wet-coupling days with AP precipitation. Mean values for AP-only samples are boldface if they differ from the corresponding all-day (parent) sample means at the 95% confidence level. Orange highlighting denotes variables for which the AP-only sample means differ significantly from their parent sample means in both dry (red) and wet coupling (blue). The sample size for each sample is given in the column header.

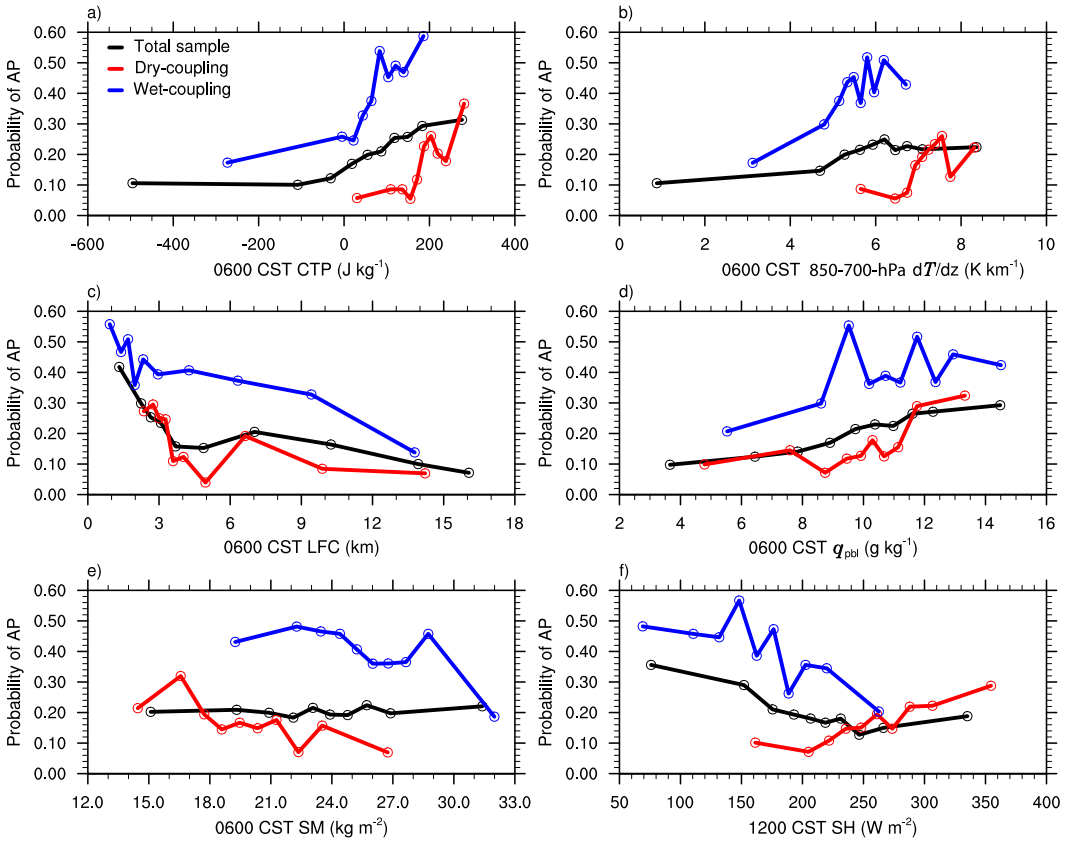

FIG. 7. The probability of same-day AP precipitation within each decile of the following six convection and LA coupling relevant variables selected from Fig. 6: (a) 0600 CST CTP, (b) 0600 CST 850–700-hPa dT/dz, (c) 0600 CST LFC, (d) 0600 CST q_{PBL}, (e) 0600 CST SM, and (f) 1200 CST SH. The red, blue, and black lines correspond to the dry coupling ($n = 713$), wet coupling ($n = 581$), and total ($n = 5424$) distributions, respectively.

AP days, 0600 CST CTP, 850–700-hPa dT/dz, and q_{PBL} tend to be higher and 0600 CST LFC tends to be lower. The directional relationship between 1200 CST SH and AP occurrence, on the other hand, is more complex. The 1200 CST SH is suppressed in wet-coupling AP days as compared to all wet-coupling days and enhanced in dry-coupling AP days as compared to all dry-coupling days. The physical underpinnings of the opposing roles of SH in AP occurrence will be made clear.

Figure 7 shows the AP probabilities for each decile of the climatological, dry-coupling, and wet-coupling range for the six variables from Fig. 6 that preceded the AP. It is important to note that although the $\mathrm{HI_{low}}$ is not included, the 0600 CST $\mathrm{HI_{low}}$, along with the CTP, is required for the coupling regime classification and differentiating between dry- and wet-coupling regimes. Figure 7a highlights a clear breakpoint at CTP $= 0\,\mathrm{J\,kg^{-1}}$, beyond which increases in CTP lead to increasing AP probability. Recall that Findell and Eltahir (2003), in their original CTP–$\mathrm{HI_{low}}$ classification framework, also deemed CTP $< 0\,\mathrm{J\,kg^{-1}}$ conditions too stable for rain. Figure 7b reveals a convenient 0600 CST 850–700-hPa dT/dz threshold of approximately $6\,\mathrm{K\,km^{-1}}$ between wet- and dry-coupling samples, consistent with that used by Frye and Mote (2010) to distinguish between synoptically benign ($<6\,\mathrm{K\,km^{-1}}$) and synoptically prime ($\geq 6\,\mathrm{K\,km^{-1}}$) conditions. Figure 7c shows that AP precipitation is most likely when the 0600 CST LFC is lower than approximately 3 km. The range of low-level specific humidity is similar for dry and wet coupling (Fig. 7d); however, elevated PBL heights (PBLH) in dry coupling likely limit the likelihood of saturation (and convective triggering) at low q_{PBL}.

There is an active debate about the preference for rain over wet versus dry soils (Ford et al. 2015b). Figure 7e shows that, climatologically, SM alone cannot explain AP probability—low-level atmospheric moisture (i.e., $\mathrm{HI_{low}}$) and instability (i.e., CTP) are required. Under dry-coupling conditions, the AP probability increases as SM decreases. Under wet-coupling conditions, the AP probability is relatively uniform across the range of SM, with the exception of a marked decline for the wettest decile ($\mathrm{SM} \geq 29\,\mathrm{kg\,m^{-2}}$). The existence of such a

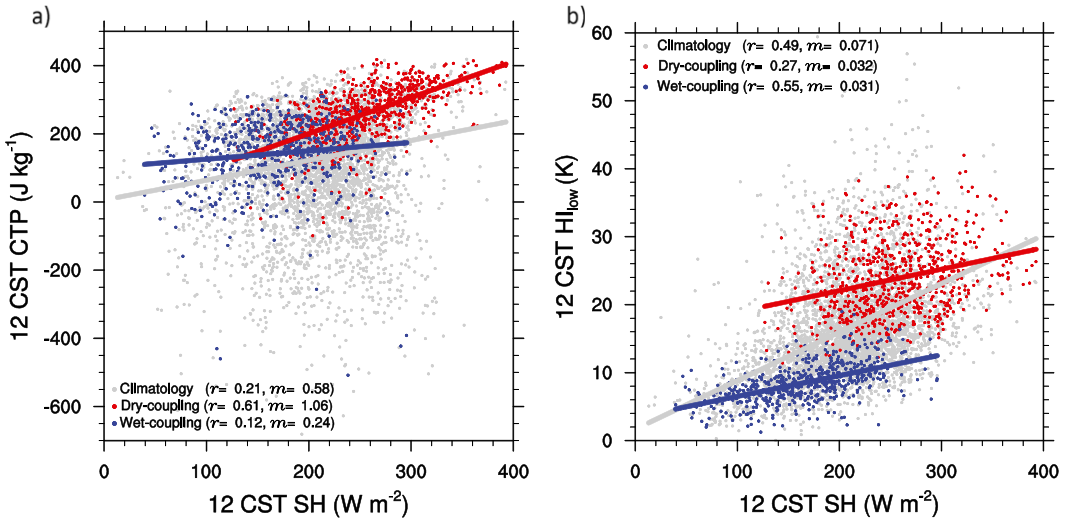

FIG. 8. Scatterplots of (a) 1200 CST SH vs 1200 CST CTP and (b) 1200 CST SH vs 1200 CST HI_{low} for all days (i.e., climatology; gray), dry-coupling days (red), and wet-coupling days (blue). Corresponding correlation coefficients and regression slopes [J kg^{-1} W^{-1} m^2 for (a) and K W^{-1} m^2 for (b)] are notated. All correlation coefficients are significant at the 95% confidence level.

breakpoint hints at a possible radiation control that will be investigated in the following section. Last, Fig. 7f reveals perhaps the most remarkable finding—that the role SH plays in AP occurrence varies directionally with coupling regime. Specifically, the probability of an AP day declines with increasing SH to a point (i.e., ~265 W m^{-2}) for wet coupling. Further increases in SH from that point in dry coupling lead to increasing AP day probability. Previously, Myoung and Nielsen-Gammon (2010) found a strong statistical relationship between SM and CIN in the SGP; dry soils can erode CIN much more efficiently than wetter soils because of increased SH (see Fig. 6; the mean value of CIN of all dry-coupling days is 240.6 J kg^{-1} and of dry-coupling days with AP is 211.3 J kg^{-1}).

d. *Radiation and soil moisture controls on AP in coupled regimes*

Figure 8 gets to the crux of how increasing SH may support AP occurrence in dry coupling and yet inhibit AP occurrence in wet coupling. In dry coupling, 1200 CST SH is strongly positively correlated (Fig. 8a; $r = 0.61$) with 1200 CST CTP and weakly correlated with 1200 CST HI_{low} (Fig. 8b; $r = 0.27$). Conversely, in wet coupling, 1200 CST SH is strongly positively correlated with 1200 CST HI_{low} (Fig. 8b; $r = 0.55$) and only weakly correlated with 1200 CST CTP (Fig. 8a; $r = 0.12$). In other words, in dry-coupling conditions, increases in SH work to trigger afternoon convection through contributing to enhanced low-level CAPE. In wet-coupling conditions, decreases in SH are related to increases in low-level moisture that lead to saturation and eventual convective triggering.

There is yet another SH–AP relationship that requires an explanation. Relative to the wet-coupling sample, wet-coupling days with AP have a reduced 1200 CST SH as well as a reduced 0600 CST SM (Fig. 6). This is an apparent contradiction if surface heat flux partitioning is primarily controlled by surface soil moisture. One hypothesis is that net available radiation (i.e., A) modifies an SH–SM relationship in wet coupling. Using scatterplots of SM and A versus SH, we test its validity (Fig. 9). Although 0600 CST SM is used in Fig. 6, in this case we use 1200 CST SM for fair comparison with 1200 CST A and 1200 CST SH. The correlation r between SM and SH in dry coupling is found to be -0.76, approximately 2 times larger than in wet coupling ($r = -0.42$; Fig. 9a). Likewise, the regression slope m between SM and SH is -11.9 W kg^{-1} for dry-coupling days and only -7.6 W kg^{-1} for wet-coupling days. The correlation between A and SH is approximately 2 times larger ($r = 0.79$) in wet-coupling conditions compared to dry coupling ($r = 0.38$). The regression slope between A and SH is 0.56 and 0.41 in wet and dry coupling, respectively. These findings indicate that dry-coupling days are in an SM-controlled (commonly known as "soil moisture limited") surface heat flux regime. Conversely, Fig. 9b shows that wet-coupling days are in a radiation (or atmosphere)-limited surface heat flux regime.

e. *Factors influencing AP intensity in coupled regimes*

Each of the variables considered in Fig. 6 was evaluated for a correlation with the AP intensity, defined as the difference between afternoon and nonafternoon precipitation. Only 0600 CST CAPE, 1200 CST SH,

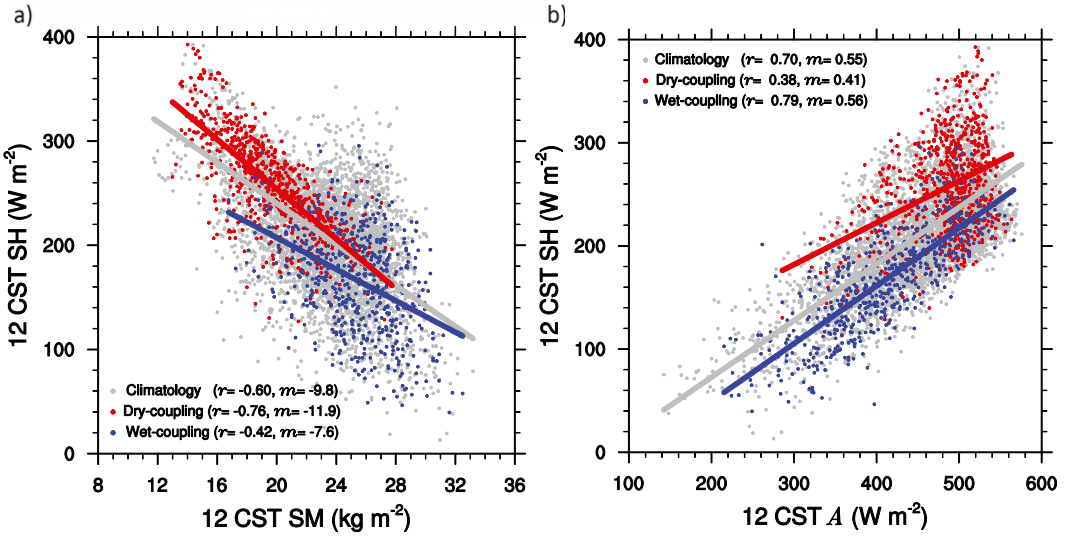

FIG. 9. Scatterplots of (a) 1200 CST SM vs 1200 CST SH and (b) 1200 CST A and 1200 CST SH for all days (i.e., climatology; gray), dry-coupling days (red), and wet-coupling days (blue). Corresponding correlation coefficients and regression slopes [W kg^{-1} for (a) and unitless for (b)] are notated. All correlation coefficients are significant at the 95% confidence level.

1200 CST EF, and 0600 CST SM were found to be significantly correlated with AP intensity (at the 95% confidence level) in both wet- and dry-coupling regimes (not shown). The focus was placed on 1200 CST SH and 0600 CST SM because of the following three considerations. First, CAPE is a total column–integrated parameter that does not specifically weight the land contribution (i.e., PBL, as does CTP), and its correlation with AP intensity in both regimes is roughly equal to that of 1200 CST EF and 0600 CST SM. Second, in both coupling regimes, the SH–AP intensity correlations are larger than EF–AP intensity correlations (dry coupling: $r = 0.19$; wet coupling: $r = 0.23$) and the LH–AP intensity correlation is insignificant in wet coupling ($r = 0.01$). Therefore, the strength of the EF–AP intensity correlation must derive from SH (not LH). Third, the concept of the LA coupling process chain begins with a perturbation of SM.

Figure 10 shows the scatterplots of 1200 CST SH and 0600 CST SM versus the difference of afternoon and nonafternoon precipitation with corresponding regression lines superimposed. In both coupling regimes, the intensity of the afternoon peak increases with decreasing SH and increases with increasing SM. The correlation strengths do not vary substantially between coupling regimes for either variable; the Pearson's correlations for the dry coupling with AP (wet coupling with AP) sample are −0.21 and 0.19 (−0.30 and 0.18) for 1200 CST SH and 0600 CST SM, respectively. What is remarkable, however, is that the regression slopes are a factor of 2.9 (0600 CST SM) to 3.7 (1200 CST SH) times larger for the wet coupling with AP sample compared to the dry coupling with AP sample.

In Fig. 8a it was shown that increases in 1200 CST SH correspond with increases in 1200 CST CTP, which in turn correspond with higher AP occurrence probability (Fig. 7a). In other words, in dry coupling, AP occurrence probability increases with increasing 1200 CST SH (Fig. 7f), but AP intensity decreases with increasing 1200 CST SH (Fig. 10a). The competing contributions of SH help to explain why the regression slopes are substantially smaller for dry than wet coupling (Fig. 10) and, relatedly, why an AP in dry coupling is difficult to discern in Fig. 4.

Under wet coupling, decreasing 1200 CST SH corresponds with both increased AP occurrence probability (Fig. 7f) and increased AP intensity (Fig. 10a). Such complimentary SH contributions may help explain the predominance of AP days in wet coupling (Figs. 4, 5). While it has been shown that SH is mainly controlled by A in the wet-coupling regime (Fig. 9b), Fig. 10b suggests AP intensity is at least partially affected by 0600 CST SM through a weaker but still significant SM control on 1200 CST SH (Fig. 9a).

4. Summary and conclusions

This study provides a detailed climatology of warm-season (May–September) LA coupling at the ARM-SGP site based on atmospheric reanalysis (NARR) and offline hydrologic model output (NLDAS-2) for the most recent 36 years (1979–2014; Fig. 1). On average, it

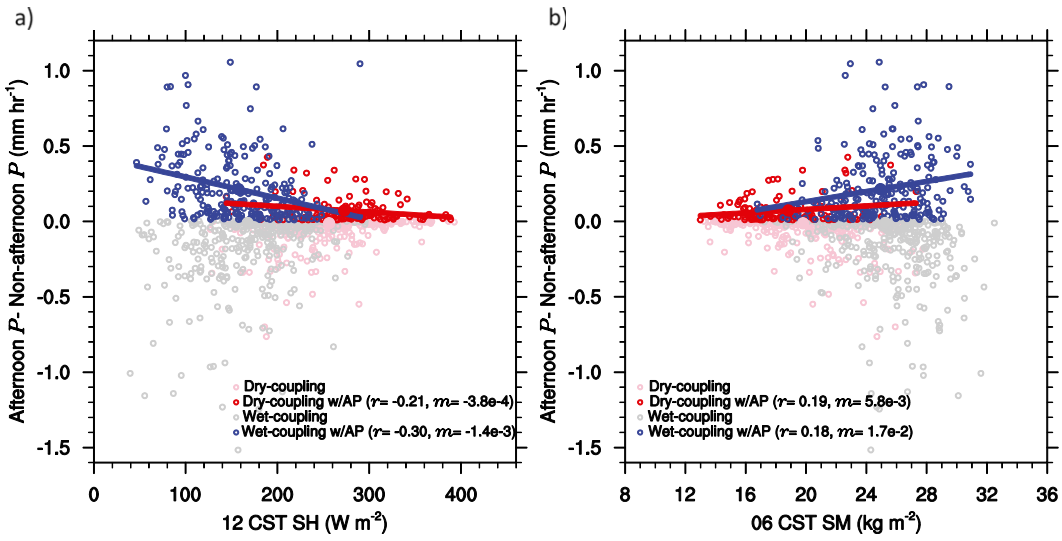

FIG. 10. Scatterplots of (a) 1200 CST SH and (b) 0600 CST SM vs the difference between afternoon P (1400–1900 CST) and nonafternoon P (0600–1300 CST Day 0 and from 2000 CST Day 0 to 0500 CST Day 1) for non-AP dry-coupling days (pink), AP dry-coupling days (red), non-AP wet-coupling days (gray), and AP wet-coupling days (blue). Large filled circles denote the composite values for AP dry- and wet-coupling samples, which fall on regression lines corresponding to each sample. Corresponding correlation coefficients and regression slopes [mm h^{-1} W^{-1} m^2 for (a) and mm h^{-1} kg^{-1} m^2 for (b)] are notated for the AP samples—all are significant at the 95% confidence level.

is shown that 16 wet-coupling and 20 dry-coupling days occur annually during the warm season. The majority of dry-coupling events occur in July and August. Wet-coupling events, on the other hand, are more uniformly distributed over the warm season but are more common in May and June. Dry-coupling events persist 0.4 days longer on average than wet-coupling events. Since 1990, there has been a marked increase (decrease) in dry (wet)-coupling frequency of 0.39 days yr^{-1} (0.45 days yr^{-1}; Fig. 1).

Analysis of the synoptic–mesoscale environments and PBL moisture budgets for wet- and dry-coupling regimes reveals the dominant role of large-scale moisture convergence in the region's precipitation. On initial consideration, it appears that wet-coupling days are a result of (zonal and meridional) moisture flux convergence over the region, dry-coupling days are a result of (zonal and vertical) moisture flux divergence, and the role of the land surface is nominal (Figs. 2, 3). However, we found that the land can play an important role in forcing anomalous afternoon peak precipitation in the region (Fig. 4). Afternoon peak precipitation is particularly more apt to occur in a wet-coupling regime and, in general, the intensity of the afternoon precipitation peak is much larger during wet-coupling events (Fig. 5).

A search for convective and LA coupling–related factors that could explain diurnal precipitation cycle phase change produced a set of six variables: convective triggering potential, 850–700-hPa lapse rate, level of free convection, 975–700-hPa layer-averaged specific humidity, sensible heat flux, and 0–10-cm soil moisture (Fig. 6). Of these six variables, only sensible heat flux and surface soil moisture were found to correlate significantly with the intensity of anomalous afternoon peak precipitation (Fig. 10). The role of sensible heat flux in afternoon peak precipitation stood out as unique among all variables considered because the directionality of the relationship varied as a function of coupling regime. In brief, the probability of afternoon peak days is directly correlated with sensible heat flux in dry-coupling conditions but indirectly correlated with sensible heat flux in wet-coupling conditions (Fig. 7f). With respect to the magnitude of the afternoon precipitation peak, decreased sensible heat flux is correlated with larger afternoon precipitation peaks in both coupling regimes, but the slope of the regression is distinctly steeper in wet coupling. Daily varying (soil or low-level atmospheric) moisture constraints on sensible heat flux in dry coupling and net available radiation constraints on sensible heat flux in wet coupling (Fig. 9; e.g., Ruiz-Barradas and Nigam 2013) are borne out in the form of subdaily variation in the diurnal precipitation phase and amplitude. It is through this lens that the role of the local land on Southern Great Plains precipitation (though more limited than that of large-scale forcing) is corroborated by our findings. In the future, the robustness

of this study's findings should be tested with other independent datasets.

Acknowledgments. This research was funded through the NYSUNY 2020 Challenge Grant Program and the University at Albany. H.-J.S. received supplemental support from the Basic Science Research Program of the National Research Foundation of Korea (NRF) funded by the Ministry of Education (2014R1A6A3A03059247). J.R. was supported by an appointment to the NASA Postdoctoral Program at the Goddard Space Flight Center, administered by Oak Ridge Associated Universities through a contract with NASA. C.F. conceived and led the study and wrote the paper. H.-J.S. performed the analysis and produced all figures. J.R. provided the land–atmosphere coupling classification dataset. All authors discussed the results and edited the paper. We thank NOAA/OAR/ESRL PSD for making NARR data freely available at http://www.esrl.noaa.gov/psd/ and NLDAS participants for providing NLDAS-2 and its forcing data at http://disc.sci.gsfc.nasa.gov/hydrology/data-holdings.

REFERENCES

Aires, F., P. Gentine, K. L. Findell, B. Lintner, and C. Kerr, 2014: Neural network–based sensitivity analysis of summertime convection over the continental United States. *J. Climate*, **27**, 1958–1979, doi:10.1175/JCLI-D-13-00161.1.

Basara, J. B., L. M. Tardif-Huber, D. X. Vanegas, B. G. Illston, C. Biradar, and W. P. Kustas, 2013: The impact of vegetation conditions on land–atmosphere interactions during an anomalously wet period. *27th Conf. on Hydrology*, Austin, TX, Amer. Meteor. Soc., 3A.4. [Available online at https://ams.confex.com/ams/93Annual/webprogram/Paper214320.html.]

Betts, A. K., 1992: FIFE atmospheric boundary layer budget methods. *J. Geophys. Res.*, **97**, 18 523–18 531, doi:10.1029/91JD03172.

——, 2004: Understanding hydrometeorology using global models. *Bull. Amer. Meteor. Soc.*, **85**, 1673, doi:10.1175/BAMS-85-11-1673.

——, 2009: Land-surface–atmosphere coupling in observations and models. *J. Adv. Model. Earth Syst.*, **1** (3), doi:10.3894/JAMES.2009.1.4.

Bonner, W. D., 1968: Climatology of the low level jet. *Mon. Wea. Rev.*, **96**, 833–850, doi:10.1175/1520-0493(1968)096<0833:COTLLJ>2.0.CO;2.

Colman, B. R., 1990: Thunderstorms above frontal surfaces in environments without positive CAPE. Part I: A climatology. *Mon. Wea. Rev.*, **118**, 1103–1122, doi:10.1175/1520-0493(1990)118<1103:TAFSIE>2.0.CO;2.

Daly, C., R. P. Neilson, and D. L. Phillips, 1994: A statistical topographic model for mapping climatological precipitation over mountainous terrain. *J. Appl. Meteor.*, **33**, 140–158, doi:10.1175/1520-0450(1994)033<0140:ASTMFM>2.0.CO;2.

——, M. Halbleib, J. I. Smith, W. P. Gibson, M. K. Doggett, G. H. Taylor, J. Curtis, and P. P. Pasteris, 2008: Physiographically sensitive mapping of climatological temperature and precipitation across the conterminous United States. *Int. J. Climatol.*, **28**, 2031–2064, doi:10.1002/joc.1688.

Dirmeyer, P. A., 2011: The terrestrial segment of soil moisture–climate coupling. *Geophys. Res. Lett.*, **38**, L16702, doi:10.1029/2011GL048268.

——, R. D. Koster, and Z. C. Guo, 2006: Do global models properly represent the feedback between land and atmosphere? *J. Hydrometeor.*, **7**, 1177–1198, doi:10.1175/JHM532.1.

——, Y. Jin, B. Singh, and X. Q. Yan, 2013: Trends in land–atmosphere interactions from CMIP5 simulations. *J. Hydrometeor.*, **14**, 829–849, doi:10.1175/JHM-D-12-0107.1.

Ek, M. B., and L. Mahrt, 1994: Daytime evolution of relative humidity at the boundary layer top. *Mon. Wea. Rev.*, **122**, 2709–2721, doi:10.1175/1520-0493(1994)122<2709:DEORHA>2.0.CO;2.

——, and A. A. M. Holtslag, 2004: Influence of soil moisture on boundary layer cloud development. *J. Hydrometeor.*, **5**, 86–99, doi:10.1175/1525-7541(2004)005<0086:IOSMOB>2.0.CO;2.

——, K. E. Mitchell, Y. Lin, E. Rogers, P. Grunmann, V. Koren, G. Gayno, and J. D. Tarpley, 2003: Implementation of Noah land surface model advances in the National Centers for Environmental Prediction operational mesoscale Eta Model. *J. Geophys. Res.*, **108**, 8851, doi:10.1029/2002JD003296.

Entekhabi, D., I. Rodriguez-Iturbe, and F. Castelli, 1996: Mutual interaction of soil moisture state and atmospheric processes. *J. Hydrol.*, **184**, 3–17, doi:10.1016/0022-1694(95)02965-6.

Erlingis, J. M., and A. P. Barros, 2014: A study of the role of daytime land–atmosphere interactions on nocturnal convective activity in the Southern Great Plains during CLASIC. *J. Hydrometeor.*, **15**, 1932–1953, doi:10.1175/JHM-D-14-0016.1.

Ferguson, C. R., and E. F. Wood, 2011: Observed land–atmosphere coupling from satellite remote sensing and reanalysis. *J. Hydrometeor.*, **12**, 1221–1254, doi:10.1175/2011JHM1380.1.

Findell, K. L., and E. A. B. Eltahir, 2003: Atmospheric controls on soil moisture–boundary layer interactions. Part I: Framework development. *J. Hydrometeor.*, **4**, 552–569, doi:10.1175/1525-7541(2003)004<0552:ACOSML>2.0.CO;2.

——, P. Gentine, B. R. Lintner, and C. Kerr, 2011: Probability of afternoon precipitation in eastern United States and Mexico enhanced by high evaporation. *Nat. Geosci.*, **4**, 434–439, doi:10.1038/ngeo1174.

Ford, T. W., A. D. Rapp, and S. M. Quiring, 2015a: Does afternoon precipitation occur preferentially over dry or wet soils in Oklahoma? *J. Hydrometeor.*, **16**, 874–888, doi:10.1175/JHM-D-14-0005.1.

——, ——, ——, and J. Blake, 2015b: Soil moisture–precipitation coupling: Observations from the Oklahoma Mesonet and underlying physical mechanisms. *Hydrol. Earth Syst. Sci.*, **19**, 3617–3631, doi:10.5194/hess-19-3617-2015.

Frye, J. D., and T. L. Mote, 2010: Convection initiation along soil moisture boundaries in the Southern Great Plains. *Mon. Wea. Rev.*, **138**, 1140–1151, doi:10.1175/2009MWR2865.1.

Gentine, P., A. A. M. Holtslag, F. D'Andrea, and M. Ek, 2013: Surface and atmospheric controls on the onset of moist convection over land. *J. Hydrometeor.*, **14**, 1443–1462, doi:10.1175/JHM-D-12-0137.1.

Guillod, B. P., and Coauthors, 2014: Land-surface controls on afternoon precipitation diagnosed from observational data: Uncertainties and confounding factors. *Atmos. Chem. Phys.*, **14**, 8343–8367, doi:10.5194/acp-14-8343-2014.

Guo, Z. C., and Coauthors, 2006: GLACE: The Global Land–Atmosphere Coupling Experiment. Part II: Analysis. *J. Hydrometeor.*, **7**, 611–625, doi:10.1175/JHM511.1.

Helfand, H. M., and S. D. Schubert, 1995: Climatology of the simulated Great Plains low-level jet and its contribution to the continental moisture budget of the United States.

J. Climate, **8**, 784–806, doi:10.1175/1520-0442(1995)008<0784:COTSGP>2.0.CO;2.

Hidalgo, H. G., and Coauthors, 2009: Detection and attribution of streamflow timing changes to climate change in the western United States. *J. Climate*, **22**, 3838–3855, doi:10.1175/2009JCLI2470.1.

Higgins, R. W., Y. Yao, E. S. Yarosh, J. E. Janowiak, and K. C. Mo, 1997: Influence of the Great Plains low-level jet on summertime precipitation and moisture transport over the central United States. *J. Climate*, **10**, 481–507, doi:10.1175/1520-0442(1997)010<0481:IOTGPL>2.0.CO;2.

Hohenegger, C., P. Brockhaus, C. S. Bretherton, and C. Schar, 2009: The soil moisture–precipitation feedback in simulations with explicit and parameterized convection. *J. Climate*, **22**, 5003–5020, doi:10.1175/2009JCLI2604.1.

Jarvinen, B. R., C. J. Neumann, and M. A. S. Davis, 1984: A tropical cyclone data tape for the North Atlantic basin, 1886–1983: Contents, limitations, and uses. NOAA Tech. Memo. NWS NHC 22, 21 pp. [Available online at http://www.nhc.noaa.gov/pdf/NWS-NHC-1988-22.pdf.]

Joyce, R. J., J. E. Janowiak, P. A. Arkin, and P. P. Xie, 2004: CMORPH: A method that produces global precipitation estimates from passive microwave and infrared data at high spatial and temporal resolution. *J. Hydrometeor.*, **5**, 487–503, doi:10.1175/1525-7541(2004)005<0487:CAMTPG>2.0.CO;2.

Koster, R. D., M. J. Suarez, R. W. Higgins, and H. M. Van den Dool, 2003: Observational evidence that soil moisture variations affect precipitation. *Geophys. Res. Lett.*, **30**, 1241, doi:10.1029/2002GL016571.

——, and Coauthors, 2004: Regions of strong coupling between soil moisture and precipitation. *Science*, **305**, 1138–1140, doi:10.1126/science.1100217.

——, and Coauthors, 2006: GLACE: The Global Land–Atmosphere Coupling Experiment. Part I: Overview. *J. Hydrometeor.*, **7**, 590–610, doi:10.1175/JHM510.1.

Kumar, S. V., C. D. Peters-Lidard, J. L. Eastman, and W. K. Tao, 2008: An integrated high-resolution hydrometeorological modeling testbed using LIS and WRF. *Environ. Modell. Software*, **23**, 169–181, doi:10.1016/j.envsoft.2007.05.012.

Kunkel, K. E., D. R. Easterling, D. A. R. Kristovich, B. Gleason, L. Stoecker, and R. Smith, 2012: Meteorological causes of the secular variations in observed extreme precipitation events for the conterminous United States. *J. Hydrometeor.*, **13**, 1131–1141, doi:10.1175/JHM-D-11-0108.1.

Lamb, P. J., D. H. Portis, and A. Zangvil, 2012: Investigation of large-scale atmospheric moisture budget and land surface interactions over U.S. Southern Great Plains including for CLASIC (June 2007). *J. Hydrometeor.*, **13**, 1719–1738, doi:10.1175/JHM-D-12-01.1.

Mather, J. H., and J. W. Voyles, 2013: The ARM Climate Research Facility: A review of structure and capabilities. *Bull. Amer. Meteor. Soc.*, **94**, 377–392, doi:10.1175/BAMS-D-11-00218.1.

Melillo, J. M., T. T. C. Richmond, and G. W. Yohe, Eds., 2014: *Climate Change Impacts in the United States: The Third National Climate Assessment*. U.S. Global Change Research Program, 841 pp., doi:10.7930/J0Z31WJ2.

Mesinger, F., and Coauthors, 2006: North American Regional Reanalysis. *Bull. Amer. Meteor. Soc.*, **87**, 343, doi:10.1175/BAMS-87-3-343.

Myoung, B., and J. W. Nielsen-Gammon, 2010: The convective instability pathway to warm season drought in Texas. Part I: The role of convective inhibition and its modulation by soil moisture. *J. Climate*, **23**, 4461–4473, doi:10.1175/2010JCLI2946.1.

Neumann, C. J., B. R. Jarvinen, C. J. McAdie, and G. R. Hammer, 1999: Tropical cyclones of the North Atlantic Ocean, 1871–1999. NOAA/NWS/NESDIS Historical Climatology Series 6-2, 206 pp.

Peters-Lidard, C. D., and Coauthors, 2007: High-performance Earth system modeling with NASA/GSFC's Land Information System. *Innovations Syst. Software Eng.*, **3**, 157–165, doi:10.1007/s11334-007-0028-x.

Pettitt, A. N., 1979: A non-parametric approach to the change-point problem. *Appl. Stat.*, **28**, 126–135, doi:10.2307/2346729.

Phillips, T. J., and S. A. Klein, 2014: Land–atmosphere coupling manifested in warm-season observations on the U.S. Southern Great Plains. *J. Geophys. Res. Atmos.*, **119**, 509–528, doi:10.1002/2013JD020492.

Rife, D. L., J. O. Pinto, A. J. Monaghan, C. A. Davis, and J. R. Hannan, 2010: Global distribution and characteristics of diurnally varying low-level jets. *J. Climate*, **23**, 5041–5064, doi:10.1175/2010JCLI3514.1.

Roundy, J. K., C. R. Ferguson, and E. F. Wood, 2013: Temporal variability of land–atmosphere coupling and its implications for drought over the southeast United States. *J. Hydrometeor.*, **14**, 622–635, doi:10.1175/JHM-D-12-090.1.

Ruane, A. C., and J. O. Roads, 2007: The diurnal cycle of water and energy over the continental United States from three reanalyses. *J. Meteor. Soc. Japan*, **85A**, 117–143, doi:10.2151/jmsj.85A.117.

Ruiz-Barradas, A., and S. Nigam, 2013: Atmosphere–land surface interactions over the Southern Great Plains: Characterization from pentad analysis of DOE ARM field observations and NARR. *J. Climate*, **26**, 875–886, doi:10.1175/JCLI-D-11-00380.1.

Santanello, J. A., M. A. Friedl, and M. B. Ek, 2007: Convective planetary boundary layer interactions with the land surface at diurnal time scales: Diagnostics and feedbacks. *J. Hydrometeor.*, **8**, 1082–1097, doi:10.1175/JHM614.1.

——, C. D. Peters-Lidard, S. V. Kumar, C. Alonge, and W. K. Tao, 2009: A modeling and observational framework for diagnosing local land–atmosphere coupling on diurnal time scales. *J. Hydrometeor.*, **10**, 577–599, doi:10.1175/2009JHM1066.1.

——, ——, and ——, 2011: Diagnosing the sensitivity of local land–atmosphere coupling via the soil moisture–boundary layer interaction. *J. Hydrometeor.*, **12**, 766–786, doi:10.1175/JHM-D-10-05014.1.

——, ——, A. Kennedy, and S. V. Kumar, 2013a: Diagnosing the nature of land–atmosphere coupling: A case study of dry/wet extremes in the U.S. southern Great Plains. *J. Hydrometeor.*, **14**, 3–24, doi:10.1175/JHM-D-12-023.1.

——, S. V. Kumar, C. D. Peters-Lidard, K. Harrison, and S. J. Zhou, 2013b: Impact of land model calibration on coupled land–atmosphere prediction. *J. Hydrometeor.*, **14**, 1373–1400, doi:10.1175/JHM-D-12-0127.1.

Seneviratne, S. I., and Coauthors, 2006: Soil moisture memory in AGCM simulations: Analysis of global land–atmosphere coupling experiment (GLACE) data. *J. Hydrometeor.*, **7**, 1090–1112, doi:10.1175/JHM533.1.

——, and Coauthors, 2010: Investigating soil moisture–climate interactions in a changing climate: A review. *Earth-Sci. Rev.*, **99**, 125–161, doi:10.1016/j.earscirev.2010.02.004.

——, and Coauthors, 2013: Impact of soil moisture–climate feedbacks on CMIP5 projections: First results from the GLACE-CMIP5 experiment. *Geophys. Res. Lett.*, **40**, 5212–5217, doi:10.1002/grl.50956.

Sheffield, J., B. Livneh, and E. F. Wood, 2012: Representation of terrestrial hydrology and large-scale drought of the continental

United States from the North American Regional Reanalysis. *J. Hydrometeor.*, **13**, 856–876, doi:10.1175/JHM-D-11-065.1.

Smith, M. B., and Coauthors, 2012: Results of the DMIP 2 Oklahoma experiments. *J. Hydrol.*, **418–419**, 17–48, doi:10.1016/j.jhydrol.2011.08.056.

Song, J., K. Liao, R. L. Coulter, and B. M. Lesht, 2005: Climatology of the low-level jet at the southern Great Plains atmospheric boundary layer experiments site. *J. Appl. Meteor.*, **44**, 1593–1606, doi:10.1175/JAM2294.1.

Stensrud, D. J., 1996: Importance of low-level jets to climate: A review. *J. Climate*, **9**, 1698–1711, doi:10.1175/1520-0442(1996)009<1698:IOLLJT>2.0.CO;2.

Stewart, I. T., D. R. Cayan, and M. D. Dettinger, 2004: Changes in snowmelt runoff timing in western North America under a 'business as usual' climate change scenario. *Climatic Change*, **62**, 217–232, doi:10.1023/B:CLIM.0000013702.22656.e8.

Sun, Y., S. Solomon, A. Dai, and R. W. Portmann, 2006: How often does it rain? *J. Climate*, **19**, 916–934, doi:10.1175/JCLI3672.1.

Taylor, C. M., and R. J. Ellis, 2006: Satellite detection of soil moisture impacts on convection at the mesoscale. *Geophys. Res. Lett.*, **33**, L03404, doi:10.1029/2005GL025252.

——, R. A. M. de Jeu, F. Guichard, P. P. Harris, and W. A. Dorigo, 2012: Afternoon rain more likely over drier soils. *Nature*, **489**, 423–426, doi:10.1038/nature11377.

Tukey, J. W., 1977: *Exploratory Data Analysis.* Addison-Wesley, 688 pp.

van den Hurk, B., M. Best, P. Dirmeyer, A. Pitman, J. Polcher, and J. Santanello, 2011: Acceleration of land surface model development over a decade of glass. *Bull. Amer. Meteor. Soc.*, **92**, 1593–1600, doi:10.1175/BAMS-D-11-00007.1.

Wei, H. L., Y. L. Xia, K. E. Mitchell, and M. B. Ek, 2013: Improvement of the Noah land surface model for warm season processes: Evaluation of water and energy flux simulation. *Hydrol. Processes*, **27**, 297–303, doi:10.1002/hyp.9214.

Westra, D., G. J. Steeneveld, and A. A. M. Holtslag, 2012: Some observational evidence for dry soils supporting enhanced relative humidity at the convective boundary layer top. *J. Hydrometeor.*, **13**, 1347–1358, doi:10.1175/JHM-D-11-0136.1.

Wetzel, P. J., S. Argentini, and A. Boone, 1996: Role of land surface in controlling daytime cloud amount: Two case studies in the GCIP-SW area. *J. Geophys. Res.*, **101**, 7359–7370, doi:10.1029/95JD02134.

Wood, E. F., Ed., 1991: *Land Surface–Atmosphere Interactions for Climate Modeling: Observations, Models and Analysis*. Kluwer Academic Publishers, 314 pp.

Xia, Y. L., and Coauthors, 2012: Continental-scale water and energy flux analysis and validation for the North American Land Data Assimilation System project phase 2 (NLDAS-2): 1. Intercomparison and application of model products. *J. Geophys. Res.*, **117**, D03109, doi:10.1029/2011JD016048.

Yang, Q., L. R. Leung, S. A. Rauscher, T. D. Ringler, and M. A. Taylor, 2014: Atmospheric moisture budget and spatial resolution dependence of precipitation extremes in aquaplanet simulations. *J. Climate*, **27**, 3565–3581, doi:10.1175/JCLI-D-13-00468.1.